International Journal of Electrical and Computer Engineering (IJECE)
Vol. 16, No. 2, April 2026, pp. 563~576
ISSN: 2088-8708, DOI: 10.11591/ijece.v16i2.pp563-576

Parametric analysis to optimize a tradeoff between the efficiency and demagnetization of line-start permanent magnet synchronous motors

Le Anh Tuan[1], Trinh Bien Thuy[2,3], Do Nhu Y.[2]
[1]School of Electrical and Electronic Engineering, Hanoi University of Industry, Hanoi, Vietnam
[2]Faculty of Electro-Mechanics, Hanoi University of Mining and Geology, Hanoi, Vietnam
[3]Faculty of Electrical and Electronic, Vietnam-Korea College, Quang Ninh, Vietnam

Article Info

Article history:

Received May 6, 2025
Revised Dec 16, 2025
Accepted Jan 15, 2026

Keywords:

Demagnetization
Efficiency
Line-start permanent magnet synchronous motor
Permanent magnet
Simulation

ABSTRACT

The line-start permanent magnet synchronous motors (LSPMSMs) have many advantages, such as high efficiency and power factor, high energy density, and the ability to line-start. Therefore, the LSPMSMs are being studied to partially replace the induction motors (IMs) currently in use. However, LSPMSMs have disadvantages, including poor starting capability, and the permanent magnets may experience irreversible demagnetization during operation. Thus, this paper uses parametric analysis method to analyze the size of the permanent magnets to optimize the efficiency of the motor while ensuring that the permanent magnets do not undergo irreversible demagnetization. A 15 kW, 2-pole LSPMSM was used for experimentation, and the results show that the motor achieves the highest efficiency of η_{max} = 95.5% at w_M = 35 mm. However, when the motor thickness w_M is greater than or equal to 34 mm, the motor experiences significant demagnetization. Thus, selecting permanent magnets (PM) size and material type that balance motor efficiency and avoid irreversible demagnetization needs careful consideration. Additionally, the experimental and simulation results are consistent, confirming the accuracy between the two methods.

Corresponding Author:

Do Nhu Y.
Faculty of Electro-Mechanics, Hanoi University of Mining and Geology
No.18 Vien Street, Duc Thang Ward, Bac Tu Liem District, Ha Noi, Vietnam
Email: donhuy@humg.edu.vn

1. INTRODUCTION

Currently, all countries have policies for energy conservation, particularly in electrical energy. The use of energy-saving and efficient practices has become increasingly urgent for sustainable development and to address the risks of depleting fossil fuel resources and environmental pollution [1]. Statistics show that electricity accounts for a significant 40% of the total energy sources used by humanity today [2]. Additionally, according to a research report from the international energy agency (IEA), electric motors and their control systems lead in electricity consumption among various types of electrical loads. Nowadays, electric motors consume approximately 70% of the electricity used in industry [3]. The high energy consumption of electric motors is due to their widespread application: electric motors are extensively used in all fields, including industry, agriculture, and daily life. They are typically installed in machinery consisting of large power devices such as machine tools, fans, conveyors, pumps, industrial production lines, and

everyday household appliances. Therefore, high-efficiency electric motors will certainly receive attention in the near future to implement the urgent energy conservation strategy.

The line-start permanent magnet synchronous motors (LSPMSMs) have been shown to have advantages, such as high efficiency, the power factor close to 1, and high torque density [4]. The LSPMSM is essentially a hybrid of a permanent magnet synchronous motor (PMSM) and an induction motor (IM). Thus, in addition to possessing the advantages of PMSMs, it also has the benefits of squirrel cage IMs, such as the ability to line-start [5]. Because of these advantages, LSPMSM is receiving attention for research and application as an effective solution to partially replace the currently popular IMs.

LSPMSMs currently have many ongoing studies aimed at enhancing the operational efficiency. The researches are quite diverse, covering various parameters of the motor, such as the application of optimization algorithms in design, improving configurations, and addressing factors that affect performance during operation. Research aimed at enhancing the efficiency of the LSPMSM includes the application of optimization algorithms to achieve the highest efficiency in design. Optimization studies typically focus on optimizing the size of the permanent magnets (PMs), the placement of the PMs, and the dimensions of the flux barriers through various methods such as lumped magnetic models [6], design of experiments (DOE) [7], particle swarm optimization (PSO) [8], Pareto-front [9], and other optimization algorithms. Research results have shown that the efficiency and power factor of the LSPMSM with optimized design are significantly higher compared to an IM of equivalent power. In addition to optimizing motor parameters, studies also focus on proposing new configurations to enhance efficiency. These proposals mainly involve design solutions for rotor configurations, including teeth, slots, dimensions of the flux barriers and PMs [10], [11]. Analysis, simulation, and experimental results indicate that the proposed configurations not only achieve high efficiency but are also simple and reliable to manufacture, using minimal permanent magnet material. Along with optimization research and the proposed configurations, studies evaluating the factors affecting LSPMSM's efficiency are also of interest. Factors influencing the operational efficiency of the LSPMSM may include the stator slot configuration [12], the operating temperature [13], and the quality of the supply voltage [14]. All studies indicate that the efficiency of the LSPMSM heavily depends on both design and operating conditions. Therefore, for the LSPMSM, attention must be given not only to the design phase but also to operational requirements to avoid adverse factors affecting efficiency. Thus, it can be seen that studies aimed at enhancing the efficiency of LSPMSM are still highly relevant today.

Although the LSPMSM has been confirmed to have advantages of high efficiency, it also has significant drawbacks that need to be addressed, specifically the risk of irreversible demagnetization of permanent magnets (PMs) during operation. The phenomenon of irreversible demagnetization affects most of the motor's operational parameters, particularly efficiency. Research aimed at preventing irreversible demagnetization of the PM is currently a focus of interest and is a key factor determining the popularity of this motor. Among the factors influencing demagnetization, the operating temperature directly affects the characteristics of the PM and can even lead to the loss of magnetism in the magnets. Therefore, at high temperatures, the likelihood of irreversible demagnetization increases [15]. This irreversible demagnetization process is more likely to occur under heavy load conditions, especially during motor startup [16]. Additionally, the operating state of the motor is also a factor that causes irreversible demagnetization. These states typically include starting, resynchronization, out-of-step fault, overload, short circuits, open phase circuits, and sudden load changes [17]. Additionally, the configuration of the motor and the PM materials used are also confirmed to influence the likelihood of irreversible demagnetization. In research, several motor configurations that enhance resistance to irreversible demagnetization have been proposed [18], [19]. Moreover, the PM materials are believed to affect demagnetization and have been studied [20]. Therefore, the phenomenon of irreversible demagnetization is one of the main drawbacks of motors using PM, and it is essential to avoid this occurrence during operation.

In summary, there are numerous studies focusing on design optimization, selecting suitable rotor configurations, and eliminating factors that affect efficiency to enhance the operational efficiency of the motor. However, the LSPMSM has the drawback of the potential for irreversible demagnetization of the permanent magnets. Due to the phenomenon of irreversible demagnetization, the motor will no longer operate according to its original specifications and may even fail to function. Furthermore, irreversible demagnetization significantly affects the motor's efficiency, leading to a decline in performance. In summary, it can be said that the greatest advantage of LSPMSMs is their high efficiency; however, the most significant issue during operation is the irreversible demagnetization of the PMs. There are many diverse studies focused on enhancing efficiency or preventing demagnetization. However, research on selecting permanent magnets in terms of size and type to ensure not only high efficiency but also to avoid demagnetization during operation is still limited. Furthermore, the choice of PMs that ensures efficiency and prevents demagnetization is crucial in the operation of LSPMSM, as these two factors are inseparable due to their direct mutual influence. Therefore, this paper studies demagnetization and the operational efficiency of the

LSPMSM. In this research, the paper applies parametric analysis and finite element analysis (FEA) methods to evaluate the efficiency and the process of irreversible demagnetization of the LSPMSM-15 kW, 2-pole. In the paper, sections 2 and 3 introduce the LSPMSM model, the demagnetization mechanism of PM, the parameters affected by demagnetization, and the selection of PM size to ensure performance requirements and theoretically avoid demagnetization. In section 4, based on preliminary theoretical calculations, the paper simulates LSPMSM, and section 5 conducts experiments on certain characteristics to confirm the consistency between theoretical, simulated, and experimental results.

2. MODEL, BACK ELECTROMOTIVE FORCE AND EFFICIENCY

2.1. Model of LSPMSM

The mathematical model of LSPMSM is described by a set of equations concerning voltage, flux, and torque. The *dq* reference coordinate system is typically used to represent the LSPMSM model. The model of the LSPMSM is represented by (1) - (3) [21],

$$\begin{cases} u_{ds} = r_1 i_{ds} + \frac{d\Psi_{ds}}{d_t} - \omega_r \Psi_{qs} \\ u_{qs} = r_1 i_{qs} + \frac{d\Psi_{qs}}{d_t} + \omega_r \Psi_{ds} \end{cases} \begin{cases} u'_{dr} = r'_{dr} i'_{dr} + \frac{d\Psi'_{dr}}{d_t} = 0 \\ u'_{qr} = r'_{qr} i'_{qr} + \frac{d\Psi'_{qr}}{d_t} = 0 \end{cases} \quad (1)$$

$$\begin{cases} \Psi_{ds} = (L_{ls} + L_{md}) i_{ds} + L_{md} i'_{dr} + \Psi'_m \\ \Psi_{qs} = (L_{ls} + L_{mq}) i_{qs} + L_{mq} i'_{qr} \end{cases} \begin{cases} \Psi'_{dr} = L'_{lr} i'_{dr} + L_{md}(i_{ds} + i'_{dr}) + \Psi'_m \\ \Psi'_{qr} = L'_{qr} i'_{qr} + L_{mq}(i_{qs} + i'_{qr}) \end{cases} \quad (2)$$

The electromagnetic torque of the LSPMSM is defined:

$$T_{el} = \frac{3}{2} p \left[\underbrace{\left(L_{md} i'_{dr} i_{qs} - L_{mq} i'_{qr} i_{ds}\right)}_{T_{ind}} + \underbrace{\Psi'_m i_{qs}}_{T_{exc}} + \underbrace{\left(L_{md} - L_{mq}\right) i_{ds} i_{qs}}_{T_{rel}} \right] \quad (3)$$

T_{ind}, T_{exc}, T_{rel} is the induction, excitation and reluctance torque; p is the number of poles.

2.2. Back-electromotive force

The back-electromotive force (B-EMF) is identified as one of the parameters that significantly affects the operating characteristics of the LSPMSM. B-EMF is the voltage measured across the terminals of the stator winding when the motor operates at synchronous speed and is no-loaded. B-EMF is determined as (4) [22]:

$$E_0 = 4.44 f w_s k_s \frac{b_{M0}.B_r.\tau_p D \alpha_p.L_{Fe}}{k_{\sigma M}} \quad (4)$$

where f is the supply frequency, w_s is the number of stator turns per phase, k_{ws} is the stator winding factor, $k_{\sigma M}$ is the leakage magnetic flux coefficient, μ_{rec} is the relative permeability of the PM, k_C is the Carter coefficient, D is the rotor outer diameter, l_{Fe} is the length of the rotor's iron core, b_{M0} is the no-load leakage flux coefficient of the PM, B_r is the remanence of PM, α_p is the pole pitch coverage coefficient of the PM.

From (4), the B-EMF value depends on the remanence of the PM. The relationship between B_r and E_0 is linear; as B_r increases, E_0 increases, and vice versa. Additionally, the B-EMF value also depends on the α_p, meaning it is influenced by the width of the flux barrier in the magnetic circuit.

2.3. Efficiency

The efficiency of the motor is the ratio of output power to input power. Additionally, efficiency is also determined by the input power consumption and the losses. In the steady-state, the power consumption of LSPMSM is determined as (5) [23]:

$$P_1 = 3\left[E_0 I_{qs} + r_1 I^2 + I_{ds} I_{qs}\left(X_{ds} - X_{qs}\right)\right] \quad (5)$$

where X_{ds}, X_{qs} are the stator synchronous reactance of d and q axes. From (5), it can be seen that the power consumption of the LSPMSM depends on the value of the B-EMF (E_0). Additionally, if we neglect the iron core losses of the stator and mechanical losses, the power losses of the motor at this point are the losses in the stator winding.

$$\Delta_p = 3r_1 I^2 = 3r_1(I_{ds}^2 + I_{qs}^2) \quad (6)$$

As a consequence, the efficiency of the motor is (7),

$$\eta = \frac{P_1 - \Delta_P}{P_1} = \frac{3[E_0 I_{qs} + r_1 I^2 + I_{ds} I_{qs}(X_{ds} - X_{qs})] - 3r_1(I_{ds}^2 + I_{qs}^2)}{3[E_0 I_{qs} + r_1 I^2 + I_{ds} I_{qs}(X_{ds} - X_{qs})]} \quad (7)$$

Thus, (7) shows that the efficiency of the motor in the steady state depends on the value of the B-EMF value. Additionally, as analyzed, the B-EMF is significantly affected by the irreversible demagnetization process. Therefore, it can be concluded that the efficiency of the motor is also greatly influenced by the demagnetization phenomenon.

3. DEMAGNETIZATION OF PM

As analyzed above, the irreversible demagnetization process significantly affects the operation of the motor, particularly it is efficiency during operation. Therefore, the operational characteristics and demagnetization mechanisms of the PM will be studied and analyzed. Additionally, in the design phase, to ensure proper operation and avoid PM demagnetization, several analytical calculations are often applied to select the preliminary dimensions of the PM.

3.1. Operating point of PM

The demagnetization curve is an important characteristic of PM, commonly used to evaluate the operating point and the level of demagnetization of the PM. There are two types of demagnetization curves commonly used [24]: the magnetic field (*BH* curve) and the magnetic field (*JH* curve). Each point on the *JH* (H_m, J_m) can be related to a corresponding point on the *BH* curve (H_m, B_m).

$$B_m = \mu_0 H_m + J_m \quad (8)$$

If the operating point of PM is within the linear region, there will be no risk of demagnetization. If the operating curve intersects the BH curve below the "knee point" of the demagnetization curve, partial irreversible demagnetization of the permanent magnet will occur. Therefore, the designer must ensure that the operating point is far from the knee region of the hysteresis curve under the worst conditions to avoid the risk of this partial irreversible demagnetization.

3.2. Demagnetization mechanism of the PM

The LSPMSM is affected by three types of magnetomotive force (MMF) during the startup process [16]. The three types are the stator current MMF F_s, the rotor current MMF F_r, and F_g is the MMF generated by the stator current due to the magnetic flux variation caused by the permanent magnet (PM). These three MMFs, along with F_{pm} generated by the PM, lead to the phenomenon of irreversible demagnetization, where the operating point of the PM is below the knee point. The worst-case scenario for irreversible demagnetization is when all the magnetomotive forces are in the opposite direction to F_{pm}. The total magnetomotive force, resulting from the combination of the four MMF F_s, F_r, F_g, and F_{pm}, is (9):

$$F = F_{pm} + F_s + F_r + F_g \quad (9)$$

The squirrel cage generates an electromagnetic shielding effect during the startup process that protects the PM from demagnetization due to the magnetic field F_δ passing through the squirrel cage bars. The impact of the protective electromagnetic shield can be determined by the depth permeability and is defined by (10) and (11):

$$B_x = B_0 e^{-(x/\Delta)} \quad (10)$$

$$\Delta = \sqrt{\frac{2}{2\pi s f_1 \mu_1 \sigma_1}} \quad (11)$$

where B_0 is the magnetic flux density at the surface of the squirrel cage bar, x is the distance between a point on the squirrel cage bar and the surface, Δ is the permeability depth, μ_1, σ_1, s, and f_1 are the permeability, conductivity, slip, and frequency, respectively. F_g is (12):

$$F_g = \frac{0.45 m w_s k_{ws} \Psi_M}{\sqrt{2} p} \frac{1}{(r_1/w_r)+L} \quad (12)$$

where X_t is the phase reactance, L is the phase inductance, ψ_M is the magnetic flux linkage generated by the PM. When starting up, R_1/ω_r is very large compared to L because at that point ω_r is zero, leading to a very large F_g. Subsequently, the value of R_1/ω_r decreases rapidly, and L plays an important role in operation. At this point, F_g is almost stable and does not change much. Thus, it can be seen that after startup, the amplitude of F_δ is significantly weakened by the electromagnetic shield, but there is still some F_δ that passes through the squirrel cage conductor, causing PM demagnetization. As a result, if the design is not adequate, irreversible demagnetization may occur during the transient processes of the motor, such as startup or out-of-step fault due to the stator current having a high value. When this irreversible demagnetization occurs, the value E_0 depends linearly on B_r; therefore, E_0 is reduced.

3.3. Calculation of the dimensions of the PMs

The volume of the PM of the motor is proportional to the output power. Therefore, the preliminary volume of the PM is selected to meet the required output power. The preliminary volume required for the PM of the LSPMSM is (13) [4].

$$V_M = \frac{2 k_{of} (1+k_{EC}) P_2}{\pi^2 \xi 2 p f B_r H_C} \quad (13)$$

where P_2 is the output power, H_c is the coercive force, k_{ocf} is the overload capacity factor, k_{fd} is the magnetization form factor, k_{EC} is the electromotive force factor, and ξ is the magnet utilization factor. On the other hand, the minimum thickness of the PM must be ensured according to the (14) to avoid irreversible demagnetization [19],

$$l_M \geq \frac{m}{2} \frac{4}{\pi} \frac{\sqrt{2} w_s k_{ws}}{2 p H_C} I_p \quad (14)$$

where l_M is the thickness of the PM in the magnetization direction, I_p is the peak current value during startup. I_p is determined when simulating the LSPMSM from the mathematical model in section 2.

4. SIMULATION RESULTS

This paper applies the finite element analysis (FEA) method to investigate the influence of the irreversible demagnetization phenomenon during startup on LSPMSM. The experimental motor in this paper is an LSPMSM 15 kW, 2-pole. The experimental LSPMSM uses NdFeBN38 with dimensions determined from the analytical calculations above. Experimental LSPMSM has the following main parameters in Table 1 and the configuration in Figure 1.

Table 1. Parameters of experimental LSPMSM

Parameters	Symbol	Value	Unit
Stator outer, inner diameter	D_{in}, D_{out}	245, 152	mm
Rotor outer and shaft diameter	D, D_t	151, 52	mm
Number of stators, rotor slots	Z_1, Z_2	36, 28	slots
Air gap length	δ	0,5	mm
Power supply voltage	U_n	380/660	V
Power supply frequency	f	50	Hz
Permanent magnet material	*NdFeN38*		

The rotor structure of the experimental LSPMSM features two poles, each with three identical PM bars. Based on the parameters of the experimental LSPMSM, using preliminary (13) and (15), the necessary volume V_M can be calculated for manufacturing, and to avoid demagnetization, l_M = 8 mm can be chosen. However, (13) and (15) are used preliminarily for initial calculations, as they apply the lumped parameter model, and the values used in the calculations are average values. In the experimental LSPMSM, each magnetic pole has three permanent magnet bars, so the degree of demagnetization for each bar may differ. Therefore, this paper investigates and evaluates the irreversible demagnetization potential for each permanent magnet bar. The simulation scenario involves dimensions where the thickness of the permanent magnet bar l_M = 8 mm, with the width w_M varying, ensuring that the volume V_M of the PM changes by no more than 10%

compared to the calculated value. Thus, the simulation scenario is executed with w_M varying from 29 to 35 mm in 1 mm increments (7 simulation steps).

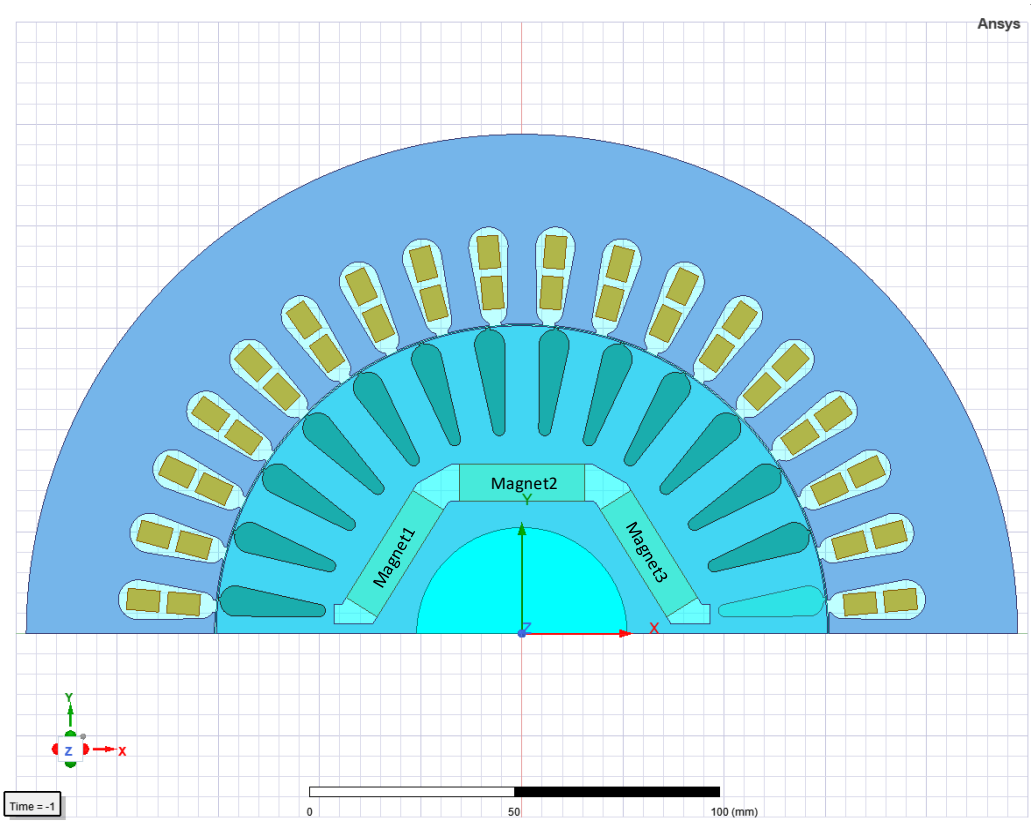

Figure 1. Configuration of LSPMSM 15 kW, 2p=2

4.1. Speed characteristics

The speed characteristic is one of the most important features in the operation of a motor. This characteristic is commonly used to evaluate the starting capability and quality. The simulation results for the startup speed characteristics of the LSPMSM in Figure 2.

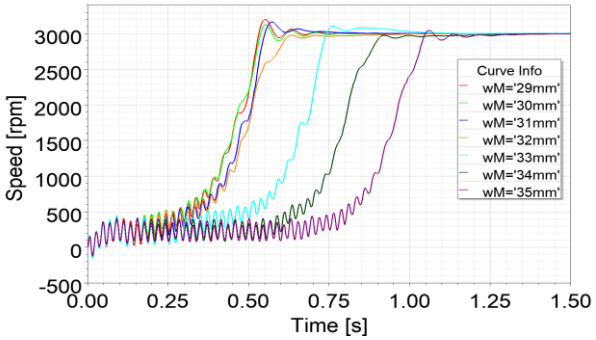

Figure 2. Speed characteristics of LSPMSM

Hence, the LSPMSM can start with a rated load at different values of w_M. However, as the width increases, starting the LSPMSM becomes more challenging. Additionally, the startup time becomes more difficult when $w_M \geq 33$ mm, at which point the motor starts with a very slow synchronization time.

4.2. Demagnetization characteristics

The paper simulates finding the operating point with the minimum flux density value (B_{min}) on each permanent magnet bar to assess the demagnetization during startup. At this B_{min}, the risk of irreversible demagnetization for the permanent magnet bar is at its highest. The simulation results for finding B_{min} for each permanent magnet bar are as Figure 3 to Figure 5.

The simulation results indicate that during the startup, magnet 1 is significantly affected by the startup current, as in Figure 3(a). As w_M increases, B_{min} decreases, meaning that the permanent magnet bar is more severely demagnetized. The smallest B_{min} of the permanent magnet bars with $w_M \geq 34$ mm approaches nearly zero, as in Figure 3(b). Thus, for $w_M \geq 34$ mm, magnet 1 is at a very high risk of experiencing irreversible demagnetization.

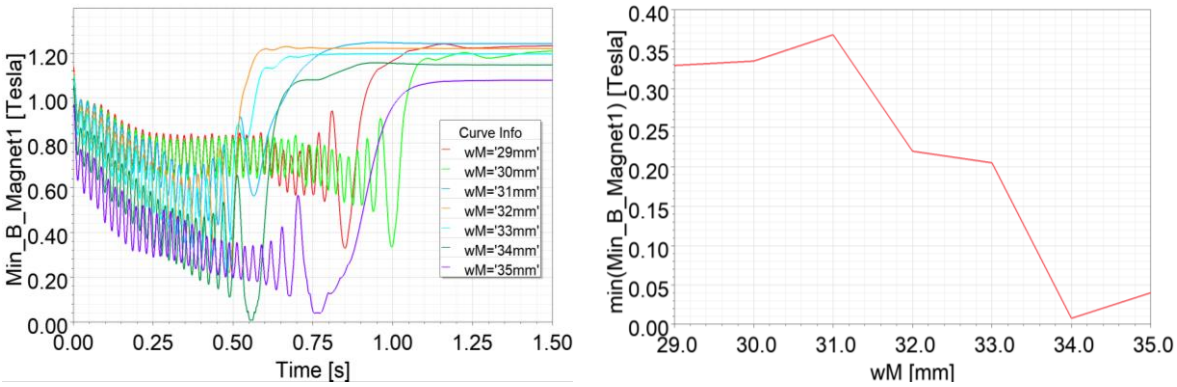

(a) (b)

Figure 3. Magnet 1 global minimum of operating point (a) B_{min} over time and (b) min (B_{min}) versus w_M

For magnet 2, the risk of irreversible demagnetization is greater compared to magnet 1. The minimum values for magnet 2 with widths equivalent to magnet 1 are significantly reduced, as shown in Figure 4(a). Similarly, in Figure 4(b) for magnet 2 with $w_M \geq 34$ mm, the lowest B_{min} is approximately zero, indicating a risk of irreversible demagnetization. Additionally, with $w_M = 35$ mm, the duration of maintaining the lowest operating point is relatively long.

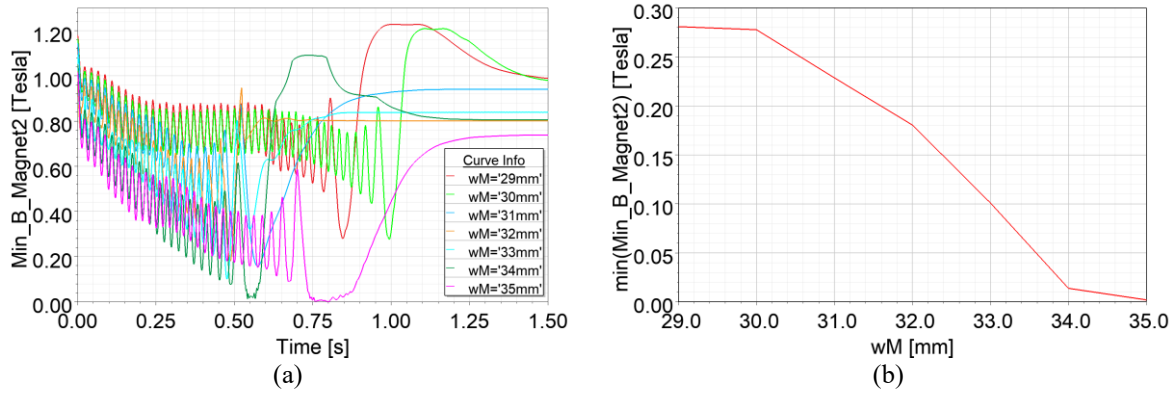

(a) (b)

Figure 4. Magnet 2 global minimum of operating point (a) B_{min} over time and (b) min (B_{min}) versus w_M

Thus, the risk of irreversible demagnetization for magnet 3 is significantly lower than that of magnets 1 and 2. The minimum B_{min} value for magnet 3 is considerably higher compared to bars 1 and 2, as shown in Figure 5(a). Similarly, in Figure 5(b) for magnet 3 with a length of $w_M \geq 34$ mm, the lowest B_{min} value is approximately zero (but still greater than the values for magnets 1 and 2). Therefore, at this point, magnet 3 still has a risk of irreversible demagnetization. Additionally, it can be noted that with $w_M = 35$ mm, the duration of maintaining the lowest operating point is similar to that of magnet 2.

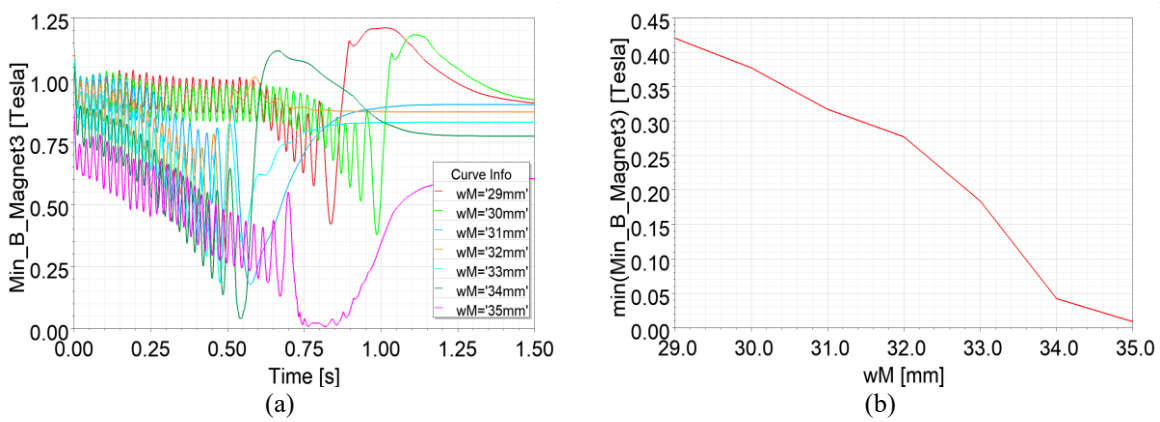

Figure 5. Magnet 3 global minimum of operating point (a) B_{min} over time and (b) min (B_{min}) versus w_M

4.3. Permanent magnet material

Material is also a significant factor affecting the irreversible demagnetization of permanent magnets. In the simulation process, the research used NdFeB-N38 material from Arnold magnetic technologies at a temperature of 20 ^{0}C. The characteristics of NdFeB-N38 are shown in Figure 6 [25].

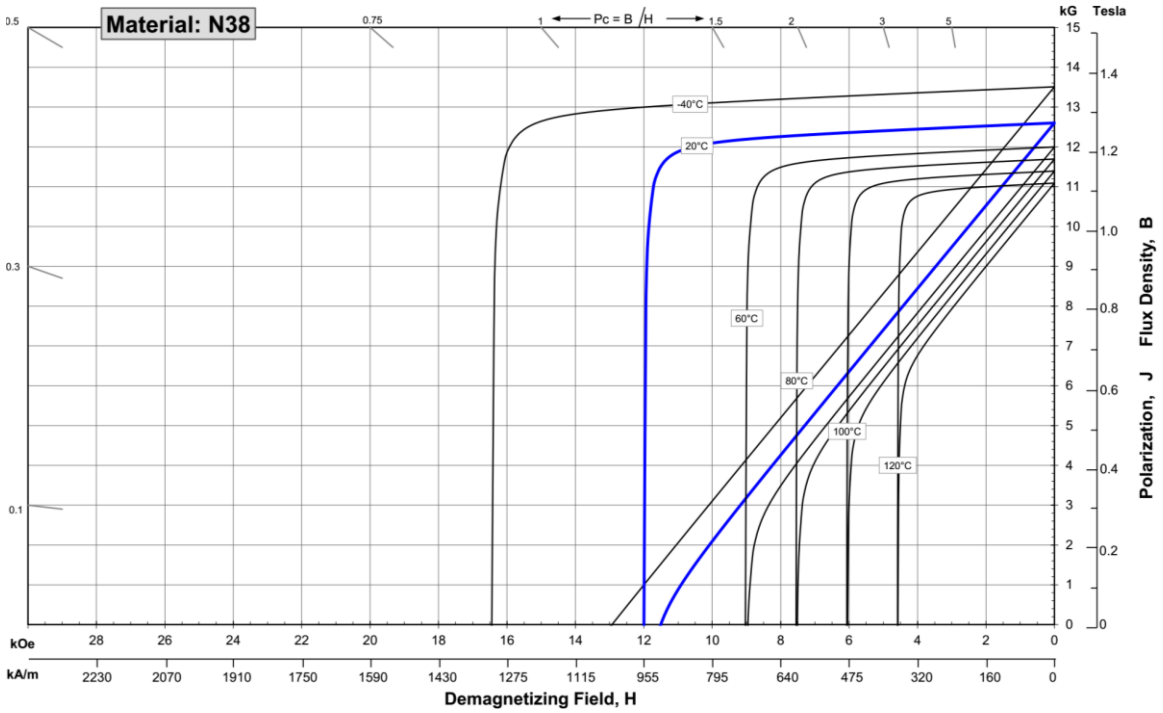

Figure 6. Demagnetization curve of NdFeB-N38 of Arnold magnetic technologies

Based on Figure 6 showing the demagnetization curve of NdFeB-N38 of Arnold Magnetic, if the motor operates at a working temperature of 20 ˚C, then when $w_M \geq 34$ mm, the B_{min} values of the magnets are all below the knee point ($B_{knee} \approx 0.05$ T). Additionally, since the demagnetization curve at 20 ˚C is nearly linear, the level of irreversible demagnetization at this temperature is not yet significant. However, it is clear that when the operating temperature of the rotor is ≥ 60 ˚C, the knee point $B_{knee} \approx 0.3$ T, and at this point, the irreversible demagnetization process will have a relatively large impact. The permanent magnets will operate with demagnetization characteristics that have a new remanence $B_{r2} < B_r$. The LSPMSM will not perform well, and its characteristics and operating parameters will be affected compared to the initial state.

4.4. Back-EMF

Back-EMF is the voltage measured across the terminals of the stator winding when no-loaded. For LSPMSM, this parameter is commonly used to assess the impact of demagnetization. The simulation results of the B-EMF waveform of the LSPMSM are shown in Figure 7.

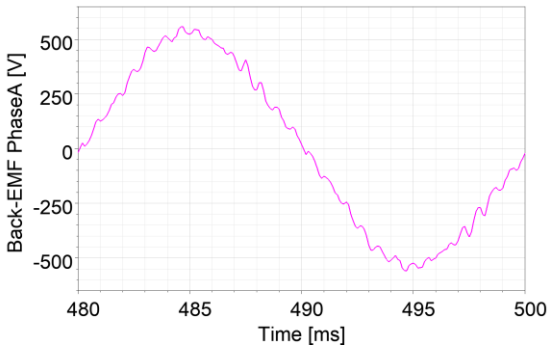

Figure 7. B-EMF waveform of LSPMSM 15 kW, 2p=2 with w_M=35mm

The amplitude of the fundamental B-EMF waveform is calculated as shown in Table 2. The simulation results are compared with the analytical calculation results introduced in section 2. The calculation results of the B-EMF value using analytical methods and the simulation with FEA show a small error. The error level is within an acceptable range between the two methods, with an error of less than 7%.

Table 2. B-EMF of experimental LSPSM

w_M (mm)	Analytical calculation	FEA calculation	Error (%)
29	323.1	346.8	6.8
30	328.4	349.1	5.9
31	330.5	351.9	6.1
32	337.2	355.8	5.2
33	342.8	358.4	4.4
34	349.6	362.2	3.5
35	355.1	365.5	2.9

4.5. Efficiency

The paper simulates the performance with different PM thicknesses to optimize the size of the PM for ensuring the efficiency and avoiding demagnetization. Additionally, the impact of demagnetization when varying PM thickness has been considered in section 4.2. The simulation scenario where w_M varies from 29 to 35 mm in 1 mm steps, the results for the efficiency of the LSPMSM in steady state are shown in Figure 8. Figure 8(a) shows the efficiency over time and the average efficiency value. In contrast, Figure 8(b) illustrates the average efficiency versus width of PM. Based on IEC/EN 60034-30-1:2014 standards for alternating current (AC) motors operating at 50 Hz and 2 poles, the efficiency values obtained in the simulations all meet the IE4 class (≥ 93.3%).

4.6. A tradeoff between the efficiency and demagnetization

The paper compiles the performance characteristics from Figure 8(b) and demagnetization characteristics from Figures 3(b), 4(b), and 5(b) based on PM thickness. This compiled characteristic serves as a basis for evaluation and finding the optimal point in selecting the PM. The graph showing the efficiency and the minimum B_{min} of the permanent magnets of the LSPMSM versus w_M is shown in Figure 9.

All w_M values within the considered limits ensure that the efficiency of the LSPMSM meets the IE4 efficiency level (≥ 93.3%). On the other hand, for the experimental 15 kW LSPMSM, choosing a larger w_M results in higher efficiency. However, it is clear that for permanent magnets, in addition to selecting the type, one must also consider the operating temperature of the magnet material. This is because temperature directly affects the demagnetization curves of the permanent magnet. Generally, electric motors are manufactured with an insulation class of *F*, with a maximum temperature tolerance of 155 ^{0}C. Therefore, to avoid demagnetization at the highest operating temperature for class F, as shown in Figure 10, in the range of

$w_M \geq 33$ mm with N38, only N38EH and N38AH can be selected. Conversely, for $w_M \leq 32$ mm, based on Figure 10, users can choose N38UH, N38EH, and N38AH. Thus, users can make their selections as shown in Table 3.

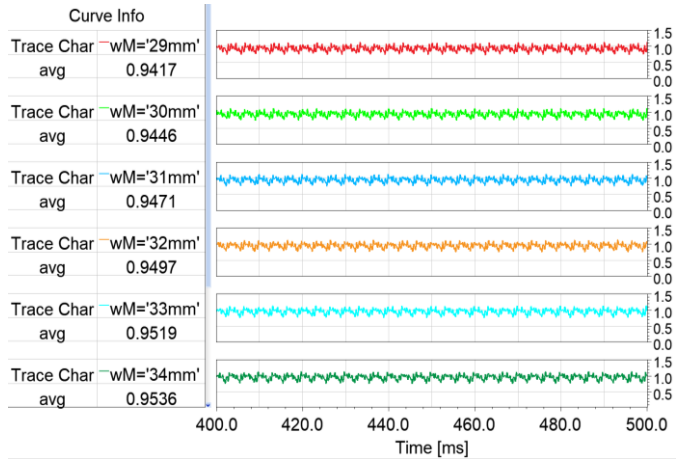

(a)

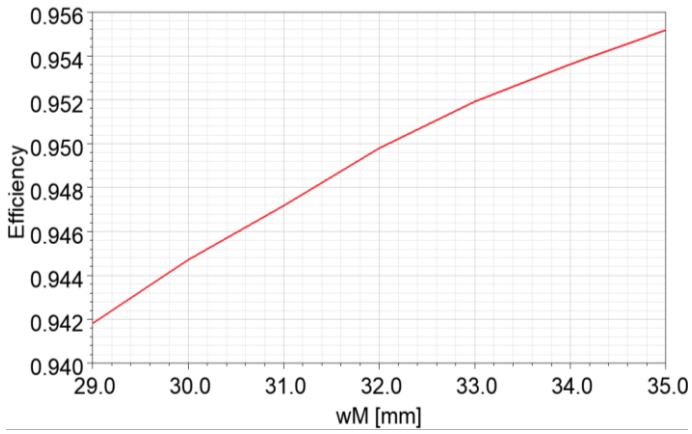

(b)

Figure 8. Efficiency in steady state (a) efficiency versus time and (b) efficiency value versus w_M

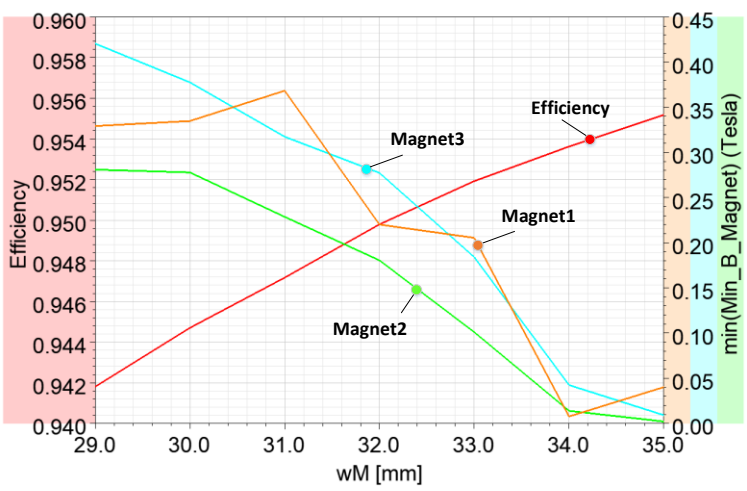

Figure 9. Efficiency and minimum B_{min} versus w_M

Table 3. Selecting permanent magnets of LSPMSM to avoid demagnetization

w_M (mm)	PM materials
≥ 33	N38EH, N38AH
≤ 32	N38UH, N38EH, N38AH

5. EXPERIMENTAL

The authors designed the LSPMSM with a permanent magnet thickness of l_M = 8 mm and selected w_M = 35 mm as the size with the highest risk of demagnetization during startup. The experimental process for the LSPMSM was conducted at Hanoi electromechanical manufacturing joint stock company (HEM), as shown in Figure 10. Figure 10(a) is the rotor of the experimental LSPMSM, while Figure 10(b) shows the coupling of the experimental motor with the testing system.

The demagnetization of the LSPMSM with two rotors corresponding to the materials NdFeN38 and NdFeN38EH. The experimental process indicated that the LSPMSM with NdFeN38 experienced irreversible demagnetization. After testing, the LSPMSM operated at an asynchronous speed, exhibiting vibration and noise, with variable working current and efficiency not meeting the design specifications.

The experimental LSPMSM with NdFeN38EH was rotated by a primary motor with open-circuit phases. A Protek 5060 oscilloscope was used to measure the voltage waveform in the phases, and the captured waveform and characteristics obtained were the B-EMF. In addition, the research conducted measurements of the efficiency of the LSPMSM. The results for measuring the B-EMF and efficiency are shown in Figure 11.

For the experimental LSPMSM with a width of w_M = 35 mm, the calculated results of B-EMF from analytical methods, simulations, and experiments are not significantly different. The simulated and experimental waveforms of B-EMF are similar Figure 11(a) and Figure 7. Thus, the experimental results demonstrate the accuracy between the analytical calculations, simulations, and experimental data of B-EMFF. The actual measurement results of efficiency value showed that the experimental LSPMSM achieved an average efficiency of 93.2% in Figure 11(b), with a difference of 2.3% compared to the simulated value in Figure 8(a). This discrepancy can be explained by the fact that some losses, such as mechanical losses, were overlooked during the simulation.

(a)

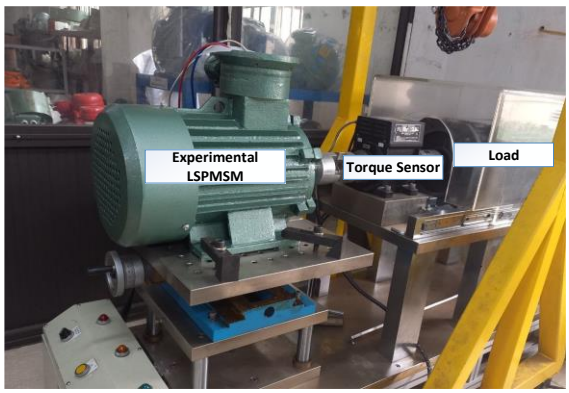

(b)

Figure 10. Testing LSPMSM 15 kW, 2p=2 (a) rotor (b) testing system

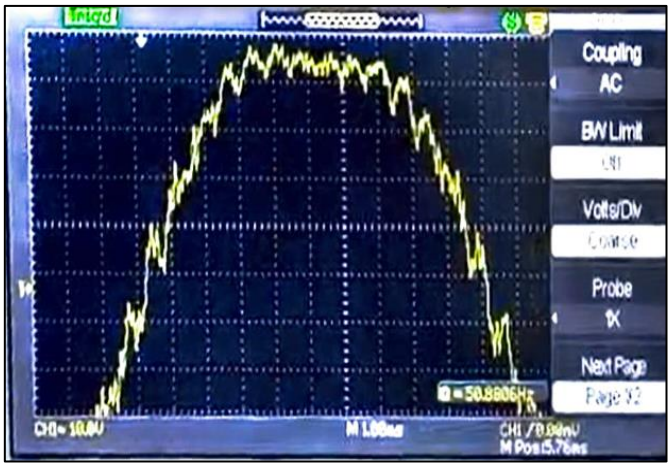

(a)

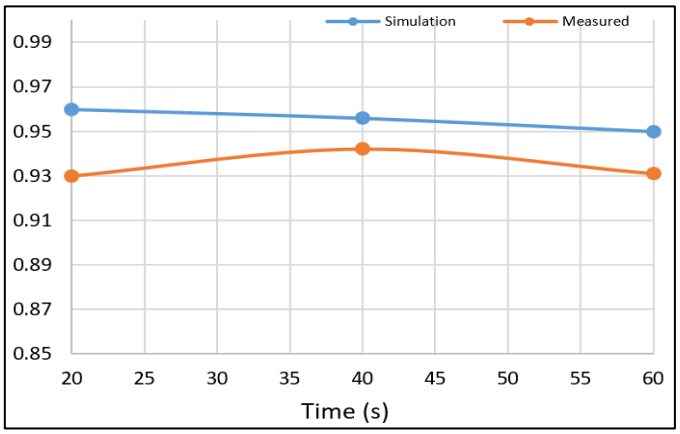

(b)

Figure 11. B-EMF wave form and efficiency in steady-state (a) B-EMF and (b) efficiency

6. CONCLUSION

The LSPMSM is currently being studied and developed to partially replace the widely used induction motors. Despite its many advantages, this motor has a significant drawback: the permanent magnets used can experience irreversible demagnetization during operation. Thus, the content of this paper investigates and proposes optimal solutions for efficiency while ensuring the avoidance of irreversible demagnetization of the permanent magnets by selecting appropriate types and sizes of permanent magnets. The content of the paper demonstrates that the research ensuring efficiency and preventing demagnetization of permanent magnets in design is entirely valid. The research results, which encompass both demagnetization and efficiency, are of great significance in the operation of LSPMSMs, as these two factors are inseparable due to their direct mutual influence. Furthermore, the findings of the paper have proven that selecting the size and material of the permanent magnets (PM) to ensure efficiency and prevent demagnetization is extremely important when designing LSPMSM. The research results also indicate that choosing PM that ensures efficiency and prevents demagnetization is highly significant in the practical operation of LSPMSM, as these two factors are inseparable due to their direct mutual influence.

The initial design choices for the LSPMSM size were based on analytical calculations. From these initial calculations, the paper applies the FEA method to simulate and investigate the parameters and characteristics of the LSPMSM. Additionally, the paper utilizes parametric analysis in conjunction with FEA to study the motor parameters. The calculated results show a good match between the analytical theory and the FEA simulation results for the experimental motor, particularly regarding the B-EMF values and the dependence of efficiency on the size of the PMs. Furthermore, the simulation results also allow users to optimally select the size and material of the magnets to achieve the best efficiency while avoiding demagnetization during startup. Based on the simulation results, the authors also constructed an experimental LPSMSM with two rotors made of different PM materials to investigate irreversible demagnetization.

The results indicate that the size of the PMs has a significant impact on irreversible demagnetization. Moreover, the choice of PM material to prevent demagnetization is extremely important. Experimental results confirm that with the standard N38 material, the motor experienced irreversible demagnetization. When irreversible demagnetization occurs, the motor's operating parameters are severely affected, and the motor no longer functions as designed. In contrast, with the heat-resistant N38EH material, the motor operates normally under various operating modes. Thus, the experimental results align with the simulation results. In addition, the research results of the paper will be the basis for selecting materials and permanent magnet sizes for LSPMSM in subsequent studies on these motors.

FUNDING INFORMATION

Authors state no funding involved.

CONFLICT OF INTEREST STATEMENT

Authors state no conflict of interest.

DATA AVAILABILITY

Data availability is not applicable to this paper as no new data were created or analyzed in this study.

REFERENCES

[1] M. Farghali *et al.*, "Strategies to save energy in the context of the energy crisis: a review," *Environmental Chemistry Letters*, vol. 21, no. 4, pp. 2003–2039, Aug. 2023, doi: 10.1007/s10311-023-01591-5.

[2] B. Lin and Z. Li, "Is more use of electricity leading to less carbon emission growth? an analysis with a panel threshold model," *Energy Policy*, vol. 137, p. 111121, Feb. 2020, doi: 10.1016/j.enpol.2019.111121.

[3] D. F. de Souza, P. P. F. da Silva, I. L. Sauer, A. T. de Almeida, and H. Tatizawa, "Life cycle assessment of electric motors: a systematic literature review," *Journal of Cleaner Production*, vol. 456, p. 142366, Jun. 2024, doi: 10.1016/j.jclepro.2024.142366.

[4] N. Do, T. Le, and X. Ngo, "Effect of permanent magnet structure on the performance of LSPMSM with a power of 22 kW and 3000 rpm," *IOP Conference Series: Earth and Environmental Science*, vol. 1111, no. 1, pp. 1–8, Dec. 2022, doi: 10.1088/1755-1315/1111/1/012047.

[5] J. Pecho and W. Hofmann, "Analysis of the effects of parameter variations on the start-up characteristics of LSPMSM," in *2019 21st European Conference on Power Electronics and Applications (EPE '19 ECCE Europe)*, Sep. 2019, p. P.1-P.10. doi: 10.23919/EPE.2019.8914800.

[6] A. Waheed and J. Ro, "Analytical modeling for optimal rotor shape to design highly efficient line-start permanent magnet synchronous motor," *IEEE Access*, vol. 8, pp. 145672–145686, 2020, doi: 10.1109/ACCESS.2020.3014718.

[7] H.-J. Park, H.-B. Hong, and K.-D. Lee, "A study on a design considering the transient state of a line-start permanent magnet synchronous motor satisfying the requirements of the IE4 efficiency class," *Energies*, vol. 15, no. 24, pp. 1–14, Dec. 2022, doi: 10.3390/en15249644.

[8] Ł. Knypiński, L. Nowak, and C. Jedryczka, "Optimization of the rotor geometry of the line-start permanent magnet synchronous motor by the use of particle swarm optimization," *COMPEL - The international journal for computation and mathematics in electrical and electronic engineering*, vol. 34, no. 3, pp. 882–892, May 2015, doi: 10.1108/COMPEL-10-2014-0276.

[9] V. Elistratova, M. Hecquet, P. Brochet, D. Vizireanu, and M. Dessoude, "Analytical approach for optimal design of a line-start internal permanent magnet synchronous motor," in *2013 15th European Conference on Power Electronics and Applications (EPE)*, Sep. 2013, pp. 1–7. doi: 10.1109/EPE.2013.6631924.

[10] B. Zöhra, M. Akar, and M. Eker, "Design of a novel line start synchronous motor rotor," *Electronics*, vol. 8, no. 1, pp. 1–18, Dec. 2018, doi: 10.3390/electronics8010025.

[11] F. Ghoroghchian, A. Damaki Aliabad, and E. Amiri, "Design and analysis of consequent-pole line start permanent magnet synchronous motor," *IET Electric Power Applications*, vol. 14, no. 4, pp. 678–684, Apr. 2020, doi: 10.1049/iet-epa.2019.0524.

[12] D. Li, G. Feng, W. Li, B. Zhang, and J. Zhang, "Effect of stator slots on electromagnetic performance of a high-voltage line-start permanent magnet synchronous motor," *Energies*, vol. 15, no. 9, pp. 1–18, May 2022, doi: 10.3390/en15093358.

[13] C. Debruyne *et al.*, "Evaluation of the efficiency of line-start permanent-magnet machines as a function of the operating temperature," *IEEE Transactions on Industrial Electronics*, vol. 61, no. 8, pp. 4443–4454, Aug. 2014, doi: 10.1109/TIE.2013.2279127.

[14] J. M. Tabora *et al.*, "Exploring the effects of voltage variation and load on the electrical and thermal performance of permanent-magnet synchronous motors," *Energies*, vol. 17, no. 1, pp. 1–16, Dec. 2023, doi: 10.3390/en17010008.

[15] M. Baranski, W. Szelag, and W. Lyskawinski, "Analysis of the partial demagnetization process of magnets in a line start permanent magnet synchronous motor," *Energies*, vol. 13, no. 21, pp. 1–20, Oct. 2020, doi: 10.3390/en13215562.

[16] D. Li *et al.*, "Irreversible demagnetization of a large capacity line-start permanent magnet synchronous motors considering influence of permanent magnet temperature," *International Transactions on Electrical Energy Systems*, vol. 2023, no. 1, pp. 1–9, Aug. 2023, doi: 10.1155/2023/6798493.

[17] T. Zawilak and C. Jędryczka, "Risk of irreversible Demagnetisation under transient states of the line start permanent magnet synchronous motor taking into account magnet temperature," *Archives of Electrical Engineering*, pp. 1107–1119, Dec. 2023, doi: 10.24425/aee.2023.147429.

[18] J.-X. Shen, P. Li, M.-J. Jin, and G. Yang, "Investigation and countermeasures for demagnetization in line start permanent magnet synchronous motors," *IEEE Transactions on Magnetics*, vol. 49, no. 7, pp. 4068–4071, Jul. 2013, doi: 10.1109/TMAG.2013.2244582.

[19] B.-H. Lee, J.-W. Jung, and J.-P. Hong, "An improved analysis method of irreversible demagnetization for a single-phase line-start permanent magnet motor," *IEEE Transactions on Magnetics*, vol. 54, no. 11, pp. 1–5, Nov. 2018, doi: 10.1109/TMAG.2018.2828507.
[20] G.-H. Kang, J. Hur, H. Nam, J.-P. Hong, and G.-T. Kim, "Analysis of irreversible magnet demagnetization in line-start motors based on the finite-element method," *IEEE Transactions on Magnetics*, vol. 39, no. 3, pp. 1488–1491, May 2003, doi: 10.1109/TMAG.2003.810330.
[21] M. H. Soreshjani, R. Heidari, and A. Ghafari, "The application of classical direct torque and flux control (DTFC) for line-start permanent magnet synchronous and its comparison with permanent magnet synchronous motor," *Journal of Electrical Engineering and Technology*, vol. 9, no. 6, pp. 1954–1959, Nov. 2014, doi: 10.5370/JEET.2014.9.6.1954.
[22] D. Stoia, O. Chirila, M. Cernat, K. Hameyer, and D. Ban, "The behaviour of the LSPMSM in asynchronous operation," in *Proceedings of 14th International Power Electronics and Motion Control Conference EPE-PEMC 2010*, Sep. 2010, pp. T4-45. doi: 10.1109/EPEPEMC.2010.5606795.
[23] V. Elistratova, "Optimal design of line-start permanent magnet synchronous motors of high efficiency," Ph.D. dissertation, Ecole Centrale de Lille, France, 2015.
[24] S. Ruoho, "Modeling demagnetization of sintered NdFeB magnet material in time-discretized finite element analysis," Ph.D. dissertation, Dept. Elect. Eng., Aalto University, New York, USA, 2011.
[25] Arnoldmagnetics, "Neodymium iron boron magnet catalog," 2017. https://www.arnoldmagnetics.com/wp-content/uploads/2017/10/Catalog-151021.pdf (accessed May 07, 2025).

BIOGRAPHIES OF AUTHORS

Le Anh Tuan received his Ph.D. degree in 2018 in Electrical Engineering from Hanoi University of Science and Technology. He is currently a lecturer in the Faculty of Energy Engineering, School of Electrical and Electronic Engineering, Hanoi University of Industry, Hanoi, Vietnam. His research areas include electric machines, electric machine simulation, power grids, power quality, and renewable energy. He can be contacted at email: tuanla1@haui.edu.vn.

Trinh Bien Thuy received a master's degree in 2014 and is currently pursuing his PhD degree in Electrical Engineering at Hanoi University of Mining and Geology. The focus of his doctoral dissertation is studying the rotor structure to enhance the working characteristics of the LSPMSM-3000 rpm motor applied in the mining industry. He can be contacted at email: Trinhthuyvhqn@gmail.com.

Do Nhu Y. received a Ph.D. in Electrical Engineering in 2013 from Tula State University, Russia. He is an Associate Professor of Electrical Engineering and currently serves as the head of the Department of Electrification and Deputy Director of the Center for Mine Electromechanical Research, as well as the head of the electrical engineering research group at Hanoi University of Mining and Geology. He is the author and co-author of numerous papers and also serves as a reviewer for several journals indexed in Scopus and ISI. His research areas include electric machines, power quality, renewable energy, and electrical networks and devices for mining. He can be contacted at email: donhuy@humg.edu.vn.